Evaluation of a Contraction Flow Field on Hydrodynamic Damage to Entomopathogenic Nematodes—A Biological Pest Control Agent

Jane P. Fife,[1] Richard C. Derksen,[2] H. Erdal Ozkan,[3] Parwinder S. Grewal,[4] Jeffrey J. Chalmers,[5] Charles R. Krause[2]

[1]Department of Food, Agricultural and Biological Engineering, The Ohio State University, 1680 Madison Avenue, Wooster, Ohio 44691; telephone: 330-263-3700, ext. 2876; fax: 330-263-3670; e-mail: fife.17@osu.edu
[2]United States Department of Agriculture, Agriculture Research Service, 1680 Madison Avenue, Wooster, Ohio
[3]Department of Food, Agricultural and Biological Engineering, The Ohio State University, 590 Woody Hayes Drive, Columbus, Ohio
[4]Department of Entomology, The Ohio State University, 1680 Madison Avenue, Wooster, Ohio
[5]Department of Chemical Engineering, The Ohio State University, 140 West 19th Avenue, Columbus, Ohio

Received 16 May 2003; accepted 16 September 2003

Published online 12 February 2004 in Wiley InterScience (www.interscience.wiley.com). DOI: 10.1002/bit.10879

Abstract: Mechanized production and delivery of biological pesticides presents challenges because the biological agents must remain viable during these processes. This study evaluates the effect of flow through an abrupt contraction, where flow characteristics similar to that found within bioprocesses and spray equipment are developed, on damage to a benchmark biological pest control agent, entomopathogenic nematodes (EPNs). An opposed-pistons, contraction flow device generated volumetric flow rates ranging between 8.26 cm^3/s and 41.3 cm^3/s. Four EPN species were evaluated: *Heterorhabditis bacteriophora*, *Heterorhabditis megidis*, *Steinernema carpocapsae*, and *Steinernema glaseri*. Damage was quantified by counting living and dead EPNs. Optical and cold field emission scanning electron microscope (CFE-SEM) images provided qualitative information to describe how the damage occurred. The experimental flow field was completely described using FLUENT, a computational fluid dynamics program. Local flow parameters computed in FLUENT were compared to EPN damage. The type and extent of damage varied between EPN species. Damaged *Heterorhabditis* spp. generally remained whole with an internal rupture located near the center of the body, while *Steinernema* spp. most often broke into several pieces. The fast-transient stress field generated at the entrance to the contraction caused a momentary tensile loading and then relaxation that damaged the EPNs. At high flow rates, the tensile stresses became large enough to cause failure of the EPN structural membrane. The relative elasticity of the EPN structural membrane may explain the differences in damage observed between the species. It is speculated that the internal rupture of the *Heterorhabditis* spp. occurred during the processes of stretching and relaxing at the contraction entrance. Appreciable damage was observed at lower average energy dissipation rates for *H. bacteriophora* (1.23E + 8 W/m^3), *H. megidis* (1.72E + 8 W/m^3), and *S. glaseri* (2.89E + 8 W/m^3) compared to *S. carpocapsae* (3.70E + 8 W/m^3). Energy dissipation rates within an equipment component should be kept below 1E + 8 W/m^3 to avoid hydrodynamic damage to EPNs. The relationship between average energy dissipation and EPN damage provides important information for future simulation efforts of actual spray equipment components. †© 2004 Wiley Periodicals, Inc.

Keywords: biopesticide; entomopathogenic nematode damage; extensional flow; tensile stress; local energy dissipation; computational fluid dynamics; *Heterorhabditis; Steinernema*

INTRODUCTION

Biological pesticides (i.e., biopesticides) are receiving increased attention as benevolent alternatives to conventional chemical pesticides (Copping and Menn, 2000). Since biopesticides are living systems (e.g., bacteria, fungi, viruses, entomopathogenic nematodes), this introduces additional challenges with respect to production, formulation, and delivery not encountered with conventional chemical pesticides. The last several decades have seen rapid advances in bioprocessing technology for the production of different microorganisms ranging from bacteria to animal

Correspondence to: Jane P. Fife

*Product and company names are necessary to report factually on available data; however, The Ohio State University and USDA neither guarantee nor warrant the standard of the product, and the use of the name by OSU or USDA implies no approval of the product to exclusion of others that may also be suitable.

Contract grant sponsors: Ohio Agricultural Research and Development Center (OARDC), Ohio State University; USDA-ARS Application Technology Research Unit

and plant cells. Yet, common to most large-scale production of these microorganisms is a stirred tank bioreactor, where mixing is typically accomplished by moving blades which deform fluid elements, the consequence of which hydrodynamic stresses are transmitted to the microorganisms within the flow field. Some biological agents are larger in size than most typically used cells, and may be more fragile and more easily damaged by hydrodynamic forces. For delivery of biopesticides, methods using existing spray technology are desirable because growers are unlikely to invest in new spray equipment or radically alter their practices (Bateman, 1999). In a conventional agricultural hydraulic spray system, the liquid suspension is pumped from a tank reservoir, through pressure regulators and flow valves, to a nozzle where the liquid suspension is forced under high pressure through an orifice to the atmosphere. The biological agents may experience a variety of hydrodynamic stresses during flow through the spray system. A better understanding of the hydrodynamic stresses within a bioreactor and spray system is required to begin identifying the equipment characteristics and operating conditions that may be least detrimental to the biological agents.

When reductions in the viability of a biological pest control agent are observed, it is generally the mechanical shear effects imposed by the equipment that are suspected to have caused the damage (Friedman, 1990; Nilsson and Gripwall, 1999). In the biotechnology literature, the term ''shear'' has been routinely used to describe any effect(s) of hydrodynamic forces on a biological material (Thomas and Zhang, 1998). In reality, most flows are a combination of shear and extensional components, which exposes the biological agents to both tangential (shear) and normal stresses. It has been hypothesized that normal forces arising from an extensional flow regime are more damaging to cells than purely shear flow at the same level of energy dissipation (Croughan and Wang, 1989; Garcia-Briones and Chalmers, 1994; Gregoriades et al., 2000; McQueen et al., 1987).

Hydrodynamic damage of animal and plant cells has been extensively studied and reviewed (Chisti, 1999; Joshi et al., 1996; Thomas and Zhang, 1998). It is well known that hydrodynamic stress can inflict damage to cells and organisms, however, published literature still lacks consistency about the ''shear'' level or nature of the damaging effects (Mardikar and Niranjan, 2000). Early studies used viscometers to quantify the shear sensitivity of cells under continuous, simple laminar-shear conditions. However, the flow field within a bioreactor or a spray system is complex (i.e., contains both shear and extensional components) and highly transient. In reality, isolation of a pure extensional flow is impossible, but flows with a high extensional component can be generated using a contraction flow device (Clay and Koelling, 1997). Recently, researchers have used either an abrupt (Gregoriades et al., 2000) or gradual (Ma et al., 2002) contraction flow device to more accurately represent the flow characteristics that cells experience in bioprocessing equipment. The flow into a contraction is geometrically simple, however, the flow field is complex with components of both shear and extension. The flow is predominately extensional in close proximity to the contraction, with pure extensional flow only along the centerline. Within a spray system, flow through a contraction is a common type of flow regime (e.g., hydraulic nozzle, valves, parts of some pumps). Thus, a contraction flow device provides a good model to evaluate the hydrodynamic effect of bioprocess and spray equipment on a biological pest control agent.

Our overall goal in this study was to evaluate the effect of flow through a contraction on the damage of a benchmark biological pest control agent, the entomopathogenic nematode (EPN). Our specific objectives were: (1) to quantitatively and qualitatively evaluate EPN damage after flow through a contraction, (2) model the flow field through the contraction using numerical methods, and (3) to compare experimental results with important flow field parameters from the model.

THEORETICAL ASPECTS

The flow field within an abrupt contraction has been well-described using numerical methods (Clay and Koelling, 1997; Gregoriades et al., 2000). The polymer coils (Clay and Koelling, 1997) and cell microcarriers (Gregoriades et al., 2000) in these studies were modeled as particles, and the suspensions were assumed to be a continuum. For modeling purposes, it is also reasonable to assume that the dilute nematode suspension is a continuum. However, because a nematode has a narrow, elongated body compared to an approximately spherical coil or cell, a more representative model of the nematode is a rod rather than a particle. Further, it is assumed that the nematodes follow streamlines with their bodies fully extended and aligned with the flow, and that there is no relative slip between the nematode and the surrounding liquid.

The current study seeks to enhance the work that has already been done on animal and plant cells by evaluating the hydrodynamic stresses (i.e., tensile and shear) developed during flow into the contraction that would act along the surface of the nematode body, a multicellular organism, to cause deformation. The stress tensor (**T**) is a mathematical operator used to describe the state of stress at any given point within a flow field. For a Newtonian fluid,

$$\mathbf{T} = -\mathrm{p}\mathbf{I} + \mu 2\mathbf{D} \tag{1}$$

where p (Pa) is the static pressure, **I** is the identity matrix, μ(kg m^{-1} s^{-1}) is the fluid viscosity, and 2**D** is the rate of deformation tensor. For two-dimensional, axisymmetric flow within a pipe, 2**D** is,

$$2\mathbf{D} = \begin{bmatrix} 2\frac{\partial \mathrm{u_r}}{\partial \mathrm{r}} & 0 & \frac{\partial \mathrm{u_r}}{\partial \mathrm{z}} + \frac{\partial \mathrm{u_z}}{\partial \mathrm{r}} \\ 0 & 2\frac{\mathrm{u_r}}{\mathrm{r}} & 0 \\ \frac{\partial \mathrm{u_r}}{\partial \mathrm{z}} + \frac{\partial \mathrm{u_z}}{\partial \mathrm{r}} & 0 & 2\frac{\partial \mathrm{u_z}}{\partial \mathrm{z}} \end{bmatrix} \tag{2}$$

where $u_r(r, z)$ (m/s) is the radial velocity component, $u_z(r, z)$ (m/s) is the axial velocity component, and r (m) and z (m)

are the radial and axial positions, respectively. Thus, for two-dimensional (2D), axisymmetric flow within a pipe, the stress components of the stress tensor [Eq. (1)] assume the following form,

$$\sigma_{rr} = -p + 2\mu\frac{\partial u_r}{\partial r}$$

$$\sigma_{\theta\theta} = -p + 2\mu\frac{u_r}{r}$$

$$\sigma_{zz} = -p + 2\mu\frac{\partial u_z}{\partial z}$$

$$\tau_{zr} = \mu\left(\frac{\partial u_r}{\partial z} + \frac{\partial u_z}{\partial r}\right) \quad (3)$$

where σ_{rr} (Pa), $\sigma_{\theta\theta}$ (Pa), and σ_{zz} (Pa) are the normal stresses in the r, θ, and z directions, respectively, and τ_{zr} (Pa) is the shear stress.

Because of its practical and theoretical appeal, the scalar quantity of energy dissipation rate has been used to characterize local hydrodynamic conditions resulting in cell damage (Gregoriades et al., 2000; Ma et al., 2002). The concept that energy dissipation can be related to cell damage was first suggested by Bluestein and Mockros (1968), and has been a common parameter used by mixing researchers to measure energy transfer within a control volume (Kresta, 1998). The rate of viscous energy dissipated (dQ_f/dt, W)per unit of volume (ΔV, m^3) for 2D, axisymmetric flow within a pipe is computed by the following equation (Schlichting, 1955).

$$\frac{dQ_f}{dt\Delta V} = \mu\left[2\left(\frac{\partial u_r}{\partial r}^2 + \left(\frac{u_r}{r}\right)^2 + \frac{\partial u_z}{\partial z}^2\right) + \left(\frac{\partial u_r}{\partial z} + \frac{\partial u_z}{\partial r}\right)^2\right] \quad (4)$$

Physically, the energy dissipation rate can be thought of as the rate of viscous energy being dissipated by the fluid element directly to a body that is in the control volume of the fluid element. It is assumed that all the viscous energy being dissipated by the fluid element will be fully realized by the body.

MATERIALS AND METHODS

Entomopathogenic Nematodes

Four species of entomopathogenic nematodes (EPNs) were studied: *Heterorhabditis bacteriophora* (Poinar) GPS 11strain, *H. megidis* (Poinar, Jackson, and Klein) UK strain, *Steinernema carpocapsae* (Weiser) All strain, and *S. glaseri* (Steiner) NJ strain. The EPNs were cultured in vivo in the laboratory using last-instar *Galleria mellonella* (L.) (Vanderhorst Canning Co., St. Mary's, OH) as the host and standard culture procedures (Kaya and Stock, 1997). The harvested EPNs (infective juvenile (IJ) stage) were placed in a 500-mL beaker, and then after 15 min the liquid from the top, which contained the dead EPNs and debris, was decanted. The concentrated suspension was then slowly poured over a tissue paper, wetted and draped over a mesh screen on top of a 150 × 20-mm petri dish to separate the living EPNs from the dead EPNs. The living EPNs swam through the tissue paper into the water below in the petri dish. The filtered suspensions were diluted with tap water to concentrations between 1000 and 2000 EPNs/mL, and 60 mL aliquots were individually stored in 150 × 20-mm petri dishes at 10°C until tests were conducted. All tests were conducted within 2 weeks following harvest.

Contraction Flow Device

An opposed-pistons, contraction flow device, developed by Clay and Koelling (1997), was used to expose the EPN suspensions to a contractional flow. The apparatus consists of two high-pressure pipes (stainless steel, diameter 1.45 cm, length 35.56 cm) (High Pressure Equipment, Erie, PA) that are coupled with an orifice plate (stainless steel, orifice diameter 0.0635 cm, plate thickness 0.1778 cm). Two pistons (stainless steel, diameter 1.44 cm) (High Pressure Equipment) are cycled in phase by a hydraulic system, so that as one piston moves forward, forcing the EPN suspension through the pipe and across the orifice, the other piston retracts at the same rate on the collection side. The stroke length of a piston is 30.48 cm. Prior to each test, the piston speed was measured using a digital tachometer (DT-107 hand digital tachometer; Shimpo, Japan), and any adjustments to the piston speed were made at this time. All tests were within 0.032 cm/s ($SE = 0.001$ cm/s) of the desired piston speed.

Immediately before conducting individual tests, the EPN suspensions were thoroughly mixed and a 10-mL sample was removed to serve as an untreated control. Approximately 50 mL of the well-mixed suspension was loaded into the pipe, between the piston and the orifice plate. Tests were conducted at piston speeds varying between 5 cm/s and 25 cm/s, corresponding to volumetric flow rates of 8.3 cm^3/s to 41.3 cm^3/s. Table I summarizes the experimental treatments. The EPN suspensions were exposed to a single pass through the contraction. Tests at each flow rate were repeated 2 times. The total time for loading, running the test, and unloading the sample was less than 10 min.

Quantification of Nematode Damage

The procedure for quantifying nematode damage is based on the commonly used practice for assessing nematode viability (Gaugler et al., 2000; Nilsson and Gripwall, 1999), where the number of living and dead nematodes within a defined sample is counted using a light microscope. Living

Table I. Experimental conditions and measured relative damage of *Heterorhabitis bacteriophora, H. megidis, Steinernema carpocapsae,* and *S. glaseri* after flow through the contraction flow device.

Piston speed (cm/s)	Volumetric flow rate (cm^3/s)	Reynolds number, inlet pipe	Reynolds number, contraction	Relative damage (%)[1,2,3]			
				H. bacteriophora	*H. megidis*	*S. carpocapsae*	*S. glaseri*
5	8.26	7.21E + 2	1.65E + 4	0.58_{aA}	0.00_{aA}	0.00_{aA}	–[4]
7	11.56	1.01E + 3	2.30E + 4	0.08_{aA}	0.15_{aA}	0.06_{aA}	–
9	14.87	1.30E + 3	2.97E + 4	0.89_{aA}	0.68_{aA}	0.43_{aA}	4.97_{aA}
11	18.17	1.59E + 3	3.63E + 4	12.00_{aAC}	1.62_{aA}	0.72_{aA}	–
13	21.48	1.88E + 3	4.29E + 4	49.65_{aBD}	20.75_{bAB}	0.71_{bA}	5.65_{bA}
15	24.78	2.16E + 3	4.93E + 4	30.47_{aBC}	30.33_{aB}	4.58_{bAB}	–
17	28.09	2.45E + 3	5.60E + 4	66.35_{aDE}	92.93_{bC}	2.53_{cAB}	56.08_{aB}
19	31.39	2.74E + 3	6.26E + 4	56.66_{aD}	79.23_{bC}	23.23_{cB}	–
21	34.69	3.03E + 3	6.92E + 4	82.76_{aEF}	89.91_{aC}	22.35_{bB}	91.60_{aC}
25	41.30	3.61E + 3	8.25E + 4	93.53_{aF}	96.12_{aC}	50.64_{bC}	–

[1]Nematode damage was quantified by counting the number of living and dead (whole and pieces) EPNs and the relative damage was computed according to Eq. (5).

[2]Means in the same row followed by the same lowercase letter do not differ significantly according to the LSD test, $P < 0.05$.

[3]Means in the same column followed by the same uppercase letter do not differ significantly according to the LSD test, $P < 0.05$.

[4]Experimental flow rates not tested for *S. glaseri*.

and dead EPNs of the infective juvenile stage are easily distinguishable from one another. All EPN species, with the exception of *S. carpocapsae*, will move in a sinusoidal manner, while *S. carpocapsae* assumes a typical J-shape, and will move when prodded. Nematodes that are dead appear to be straight and do not move.

For each treated suspension, the suspension was thoroughly mixed and a 100-μL subsample was collected with a microdispenser and added to approximately 10 mL of water in a 55 × 10-mm petri dish to allow easy viewing with the light microscope (Model DMIL, Leica, Germany), with 50× magnification. Three subsamples per replication were evaluated for all treatments. To insure that the nematodes were completely viable to start, a 100-μL sample of the untreated control was also assessed for each treatment. The mean viability of the untreated controls was 99.76% (SE = 0.05%).

Because of the nature of the tests conducted, some nematodes were damaged and remained whole, and some were broken into pieces. A procedure was developed in a previous study (Fife et al., 2003) that categorizes the damaged nematodes into three size groups, whole, halves and quarters, to provide a count for the total dead (i.e., damaged). A damaged whole nematode is defined as a dead, intact nematode that is either completely whole or has a tip from one end broken off. A half piece is defined as a completely broken portion that is approximately the length of one-half of a nematode, and a quarter piece is a discernibly smaller broken portion that is approximately the length of one-quarter of a nematode. Anything smaller, where it was not clear whether it was a true piece or internal matter that may have leaked out, was not included in the count. Nematode relative damage (RD, %) was determined by separately recording the number of live (L), damaged whole (D), half pieces (HP), and quarter pieces (QP) of EPNs within each subsample, and was computed by the following equation.

$$RD = 100 - \left(\frac{L}{L + D + \frac{HP}{2} + \frac{QP}{4}} \right) \times 100 \qquad (5)$$

Appreciable EPN damage is defined as (RD + standard error of the mean) >15% (Fife et al., 2003).

The physical damage to nematodes was observed in greater detail using a cold field emission scanning electron microscope (CFE-SEM) (Hitachi Model S-4700, Nissei Sangyo Instruments, Inc. Mountain View, CA). The specimen holder or stub used in the CFE-SEM was prepared by placing a droplet of the treated nematode suspension, approximately 100 μL, onto the stub. After the water had naturally evaporated from the stub surface, the prepared stub was examined with the CFE-SEM at an accelerating voltage of 10 kV, working distance of 21.3 mm, and 600× magnification.

Modeling of Flow Field

The flow field was modeled using FLUENT (Version 5.5, FLUENT Inc., Lebanon, NH), a computational fluid dynamics program, and using similar techniques as Gregoriades et al. (2000). The 3D contraction flow device was reduced to a 2D model because of the axisymmetric nature of the flow. Also, because of symmetry about the centerline, the 2D model was further reduced to one-half of the pipe domain to save computational effort. The computational grid used in the FLUENT simulations is presented in Figure 1. Because of differences in the dimensions of the device components in the current study

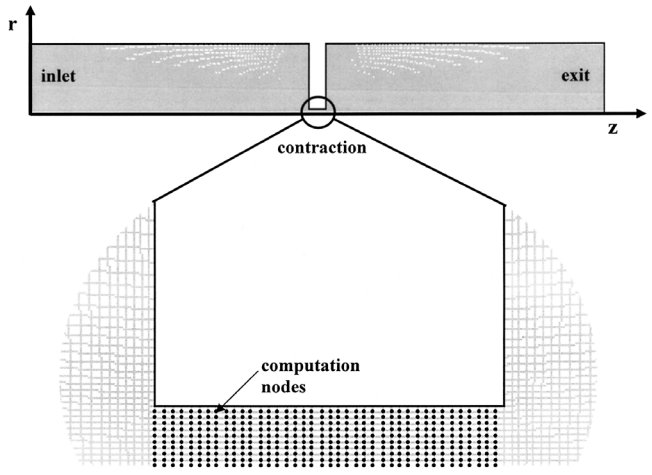

Figure 1. Grid-node locations of the experimental contraction flow device used for FLUENT simulations.

(i.e., an approximately 23:1 contraction) compared to Gregoriades et al. (2000) (i.e., 20:1 contraction), the two models were slightly different. In addition, Gregoriades et al. (2000) used a Gaussian Windows Adaptive (GWA) method to process the irregularly distributed velocity vectors from FLUENT to approximate the velocity fields located on regularly spaced node points. The GWA method was not used in the current study because the grid nodes were by design uniformly spaced within the contraction region, making the additional effort to further process the FLUENT results unnecessary. Thus, the flow field information was obtained directly from the FLUENT simulation results.

The entry and exit regions were modeled as two pipe diameters in length (2.90068 cm). The radius and length of the contraction were 0.03175 cm and 0.1778 cm, respectively. Different grid node densities along the entry and exit and within the contraction region were evaluated until a grid independent solution was obtained. The highest concentration of grid nodes was located in the contraction region, where the velocity and pressure gradients were the largest. A total of 14,800 nodes were used in the model. Within the contraction, the grid node density was 70,857 nodes/cm^2, the grid height (31.75 μm) was in the same scale as the width of an EPN, and the grid width (44.45 μm) was over an order of magnitude less than the length of an EPN.

The assumptions for this problem were standard (i.e., incompressible fluid, no slip along the walls, fluid is a continuum). The source of energy for the fluid movement is the motion of the piston. With respect to the flow field directly in front of the piston, 99% of a fully developed flow is achieved one-piston diameter in front of the piston (Tadmor and Gogos, 1979). Thus, for the majority of the pipe length upstream from the contraction the flow is fully developed. For several of the experimental conditions (Table I), the Reynolds numbers within the inlet pipe were greater than 2300, the critical Reynolds number for transition from laminar to turbulent flow in a pipe. However, as has been discussed previously (Gregoriades et al., 2000), flows that are free of an upstream disturbance and have a smooth pipe surface, which is representative of the experimental conditions, have been found to maintain laminar pipe flow at Reynolds numbers exceeding 10^4 (Schlichting, 1955). Thus, the assumption of laminar flow within the pipe for the range of experimental conditions is reasonable. Within the contraction, the Reynolds numbers exceed 10^4 (Table I). At small distances from the contraction entrance, a boundary layer will grow in the same way as it would along a flat plate at zero incidence (Schlichting, 1955). The Reynolds number at the trailing edge of the contraction for the largest flow rate tested is 2.3E + 5. Because this value is less than 3.2E + 5, the critical Reynolds number at which the boundary layer becomes turbulent along a flat plate (Schlichting, 1955), it can be assumed that all the experiments were conducted in the laminar regime within the contraction. The model solution was verified by checking the velocity profile upstream from the contraction in the simple shear region with values computed from the Hagen-Poiseuille equation.

Simulations of the contraction flow field were conducted for each of the experimental flow rates. User-defined functions were created in FLUENT to compute the stress

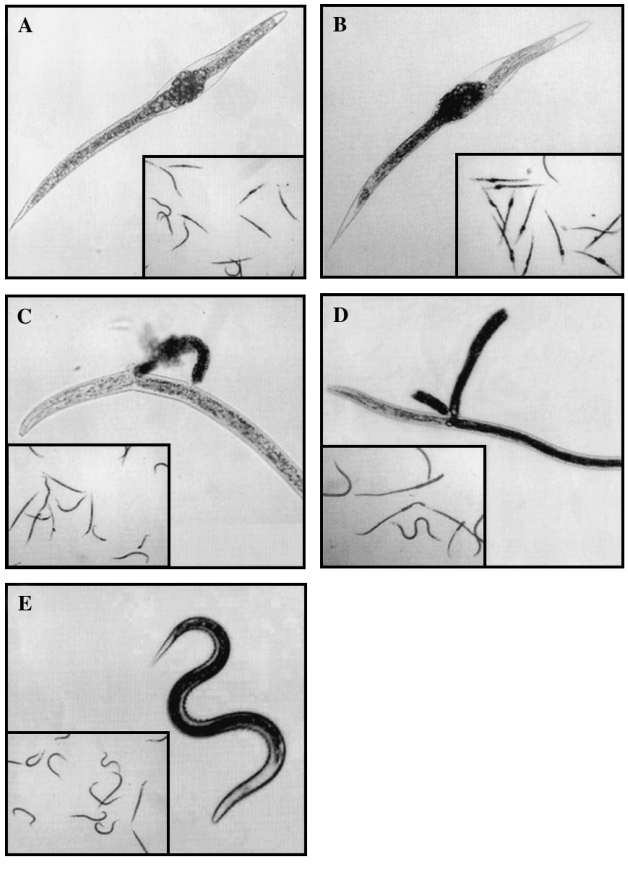

Figure 2. Representative damage observed for *Heterorhabditis bacteriophora* (A), *H. megidis* (B), *Steinernema carpocapsae* (C), and *S. glaseri* (D) after flow through the contraction, and an example of undamaged *H. bacteriophora* (E).

tensor components [Eq. (3)] and the energy dissipation rate [Eq. (4)] from the flow field information. Values of the stress tensor components and energy dissipation rates were obtained from several stream function lines [0 kg/s (center streamline), 1E-4 kg/s, 1E-3 kg/s, and 2E-3 kg/s] within the simulated flow field.

The maximum tensile force that an EPN would have experienced during flow along the center streamline was computed by multiplying the maximum center streamline tensile stress (σ_{zz}) by the cross-sectional area of the EPN cuticle, the load-bearing membrane of the nematode body. The EPN cuticle thickness was assumed to be 0.07 times the nematode diameter (Wilson et al., 2001). The tensile loading was computed for each of the EPN species for the experimental conditions where appreciable damage (i.e., >15%) started to occur. Also, for these same conditions, the total pressure change acting along the length of each EPN species was determined, where the EPN tail was taken to be at the point of maximum total pressure along the center streamline.

The mean energy dissipation rate for each experimental condition was determined by averaging the energy dissipation rate values from the computation nodes within the contraction. The highlighted computation nodes in Figure 1 indicate the locations of the energy dissipation rate values that were used to calculate the average, a total of 400 data points. The energy dissipation rate values from nodes located on the contraction wall were not included in the mean calculation for two reasons. First, the energy dissipation rates right at the wall come from flow field information that takes into account the grid area of one-half the distance from the wall to the first row of computation nodes. Within this region right next to the wall, the velocity gradient $\partial u_z/\partial r$ is extremely large due to the assumption of no-slip at the wall (i.e., the u_z velocity goes from a large value to zero at the wall). Consequently, this makes the energy dissipation rate right at the wall considerably higher compared to values within the first row of nodes away from the wall. Second, it is unlikely that a nematode will be flowing on a streamline right next to the wall. The half-distance between the wall and the first row of nodes is 16 μm. The nematode widths range between 23 and 43 μm (Poinar, 1990). Although it is possible that a portion of the nematode body could have experienced flow right next to the wall, it is more likely that the nematode did not. Based on the above discussion, it is reasonable to exclude the energy dissipation rates right at the wall to provide an average value within the contraction that is more meaningful in terms of describing the flow conditions that the nematodes were likely to have experienced. The average energy dissipation rate for each experimental condition was compared to the corresponding relative damage of each EPN species.

Figure 3. Cold field emission scanning electron microscope (CFE-SEM) micrograph of a damaged *Heterorhabditis bacteriophora* after flow through the contraction at a volumetric flow rate of 24.78 cm^3/s, which shows a region of deformation (i.e., necking) near the center of the nematode body.

Statistical Analyses

Data on nematode relative damage was analyzed by a completely randomized, 4 × 10 factorial ANOVA with subsampling, and EPN species and flow rate treatment effects. The treatment, experimental error, subsampling error, and total sum of squares were computed using a spreadsheet. The treatment interaction sum of squares was determined from the residual. Least significant differences were used to compare individual treatment means at a significance level of 0.05.

Table II. The total count of living (*L*), damaged whole (*D*), and damaged half pieces (*HP*) and quarter pieces (*QP*) of *Heterorhabditis bacteriophora, H. megidis, Steinernema carpocapsae* and *S. glaseri* after treatment for several representative experimental conditions.

	Total count of treated EPNs[a]															
	H. bacteriophora				*H. megidis*				*S. carpocapsae*				*S. glaseri*			
Volumetric flow rate (cm^3/s)	*L*	*D*	*HP*	*QP*	*L*	*D*	*HP*	*QP*	*L*	*D*	*HP*	*QP*	*L*	*D*	*HP*	*QP*
14.87	835	9	0	0	604	4	0	0	797	3	1	0	427	6	10	38
21.48	439	378	22	25	471	123	7	6	735	4	1	3	308	8	3	37
28.09	158	335	5	21	31	379	24	45	660	13	5	9	160	12	272	220
34.69	159	484	103	340	36	167	85	463	461	14	82	315	25	1	140	775

[a]Total count comes from the summation of the raw experimental data, three subsamples per replication and two replications per treatment ($n = 6$).

Entomopathogenic Nematode Damage Analysis

The observed mean relative damage of each EPN species with respect to the flow treatments is summarized in Table I. From the analysis of variance, differences in relative damage among the EPN species ($P < 0.001$), among flow rate treatments ($P < 0.001$), and for a treatment interaction ($P < 0.01$) were all found statistically significant. For volumetric flow rates $\leq$18.17 cm^3/s, the mean treatment differences between the EPN species were insignificant. At higher volumetric flow rates ($\geq$24.78 cm^3/s), *S. carpocapsae* had significantly less relative damage than the other EPN species, and, in general, *H. bacteriophora*, *H. megidis*, and *S. glaseri* were not significantly different from one another. Appreciable damage was observed at volumetric flow rates of 18.17 cm^3/s for *H. bacteriophora*, 21.48 cm^3/s for *H. megidis*, 28.09 cm^3/s for *S. glaseri*, and 31.39 cm^3/s for *S. carpocapsae*.

Representative images of damaged EPNs of each species after flow through the contraction, along with an example of undamaged *H. bacteriophora*, are presented in Figure 2. The observed nematode damage was different for *Heterorhabditis* nematodes compared to *Steinernema*. Damaged *H. bacteriophora* (Fig. 2A) and *H. megidis* (Fig. 2B) generally remained whole with an internal rupture located near the midpoint of the body or slightly off-center. However, in some cases, particularly at high volumetric flow rates ($\geq$34.69 cm^3/s), broken pieces, approximately halves and quarters, were observed in addition to the damaged whole nematodes. Figure 3 presents a more detailed CFE-SEM image of the damage to a *H. bacteriophora* nematode after treatment at a volumetric flow rate of 24.78 cm^3/s. An undamaged EPN will have parallel longitudinal ridges along

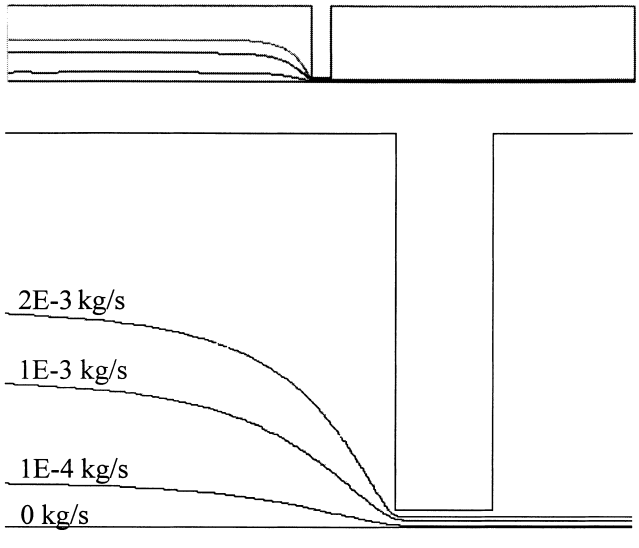

Figure 4. FLUENT generated contour plot of the stream functions 0 kg/s (center streamline), 1E-4 kg/s, 1E-3 kg/s, and 2E-3 kg/s within the experimental contraction flow device at a volumetric flow rate of 24.78 cm^3/s.

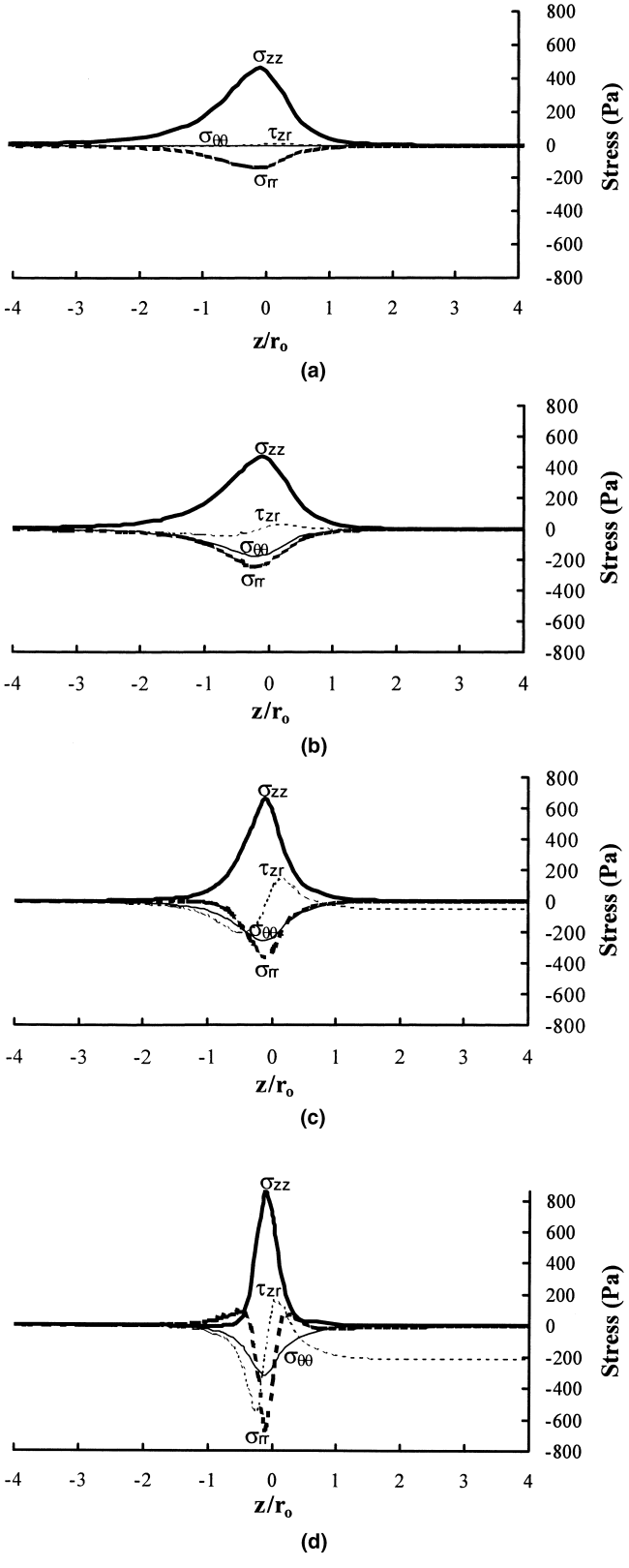

Figure 5. Stress tensor components from FLUENT simulations at a volumetric flow rate of 24.78 cm^3/s for the stream functions (a) 0 kg/s (center streamline), (b) 1E-4 kg/s, (c) 1E-3 kg/s, and (d) 2E-3 kg/s. The static pressure was removed from the normal stress components (σ_{zz}, σ_{rr}, $\sigma_{\theta\theta}$).

Table III. The average EPN sizes and the computed maximum tensile forces and pressure changes experienced by the nematodes during flow along the central streamline for the experimental conditions when appreciable damage (i.e., >15%) started to be observed for *Heterorhabditis bacteriophora, H. megidis, Steinernema carpocapsae,* and *S. glaseri.*

EPN species	Average EPN length (μm)[a]	Average EPN width (μm)[a]	Computed maximum center streamline tensile force (N)	Computed maximum center streamline pressure change (kPa)
H. bacteriophora	588	23	1.22E-4	184
H. megidis	768	29	2.72E-4	258
S. carpocapsae	558	25	4.32E-4	547
S. glaseri	1130	43	1.02E-3	460

[a]Average EPN lengths and widths from Poinar (1990).

its cuticle. Keeping this in mind, there are two apparent regions of damage. At the top of the CFE-SEM micrograph, there is a protrusion, which designates the internal rupture seen in Figure 2A and 2B. Below the protrusion, there is a slightly indented and deformed region (i.e., neck) that is located approximately at the center of the body. This ''necking'' phenomenon was not observed at all for *Steinernema*. Instead, damaged *S. carpocapsae* (Fig. 2C) and *S. glaseri* (Fig. 2D) were in most cases broken into pieces, approximately halves and quarters, and when damaged whole nematodes were observed the cuticle had been broken such that the internal matter leaked out. Table II summarizes the total counts of living and damaged (whole, halves, and quarters) nematodes of each EPN species at several representative flow rates.

Computer Simulations

Streamline contours of the modeled flow field generated in FLUENT for the experimental volumetric flow rate of 24.78 cm^3/s are presented in Figure 4, and are representative of results obtained for the range of experimental conditions. The parallel streamlines flow radially inward into the contraction, as expected for a Newtonian fluid in laminar flow. The streamlines remain parallel through the contraction and within the jet immediately after the contraction.

The stress tensor components [Eq. (3), with the static pressure removed from σ_{rr}, $\sigma_{\theta\theta}$, σ_{zz}] are presented in Figure 5A–D for the stream functions 0 kg/s (center streamline), 1E-4 kg/s, 1E-3 kg/s, and 2E-3 kg/s, respectively, for the volumetric flow rate 24.78 cm^3/s. The axial coordinates were normalized with the contraction radius (r_o), and the origin is defined as the leading edge of the contraction. Negative dimensionless axial coordinates represent locations upstream from the contraction. The strong uniaxial, extensional flow along the center streamline results in a rapid increase in tensile stress (σ_{zz}) in the axial direction and compressive stress (σ_{rr}) in the radial direction. The shear stress (τ_{zr}) is near zero and there is no normal stress in the θ-direction ($\sigma_{\theta\theta}$) along the center streamline. These simulation results (Fig. 5a) support the assumption of pure extensional flow along the center streamline. As the streamlines get further away from the center streamline (i.e., larger stream function values) (Fig. 5b–d), the shear stress becomes increasingly more pronounced and there is now a normal stress component in the θ-direction. The maximum normal tensile stress (σ_{zz}) and compressive stress (σ_{rr}) also increase in value. The normal stress component

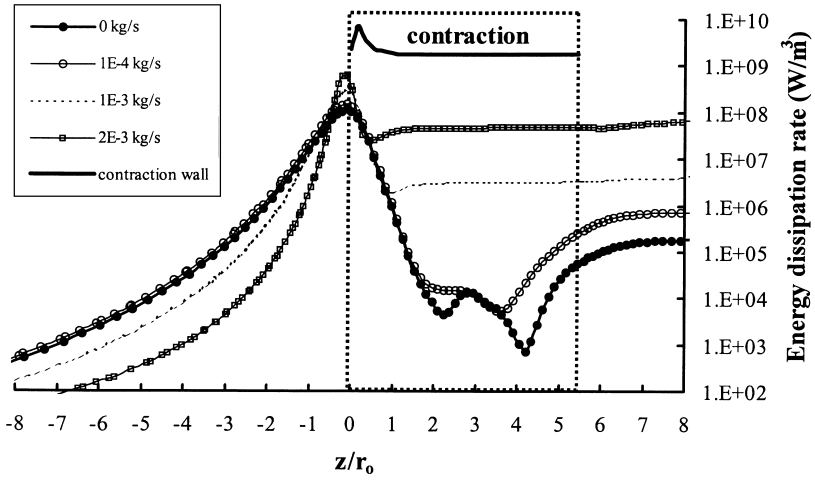

Figure 6. Energy dissipation rates computed in FLUENT at a volumetric flow rate of 24.78 cm^3/s for the stream functions 0 kg/s (center streamline), 1E-4 kg/s, 1E-3 kg/s, and 2E-3 kg/s. The location of the contraction is designated by •••••.

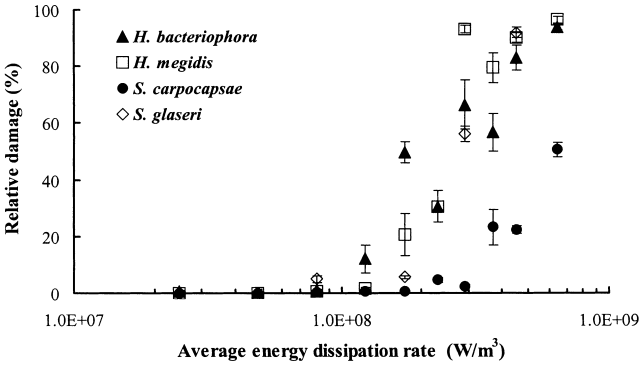

Figure 7. The measured relative damage of *Heterorhabditis bacteriophora*, *H. megidis*, *Steinernema carpocapsae*, and *S. glaseri* as a function of the average energy dissipation within the contraction from FLUENT simulations. Error bars represent standard error of the mean ($n = 6$).

maximum values and the point of inflection for the shear stress component all occur approximately 0.1 r_o upstream from the contraction entrance.

The maximum center streamline tensile loading and change in total pressure acting along each of the EPN species are presented in Table III for the experimental conditions when appreciable damage started to be observed. Comparison of the computed tensile forces between EPN genera shows that for *Heterorhabditis* spp. appreciable damage started to occur at lower tensile forces than for *Steinernema* spp. ($P = 0.1$), although the difference was not significant.

The energy dissipation rates computed in FLUENT for the experimental volumetric flow rate of 24.78 cm^3/s are presented in Figure 6. The maximum energy dissipation rates occur just inside the contraction entrance, along the contraction wall, where high shear rates (i.e., large values of $\partial u_z/\partial r$) exist. Just upstream from the contraction entrance($z/r_o = -0.1$), there is a region of high-energy dissipation due to extensional flow contributions. For streamlines within the central flow region (i.e., $\leq$1E-4 kg/s), where shear contributions are minimal, the extensional flow component ($\partial u_z/\partial z$) dominates the energy dissipation equation [Eq. (4)]. Further away from the central flow region, shear contributions are present, which increases the peak energy dissipation rates slightly. Once inside the contraction, the extensional component of the energy dissipation rapidly decreases. However, the shear component of the flow keeps the energy dissipation rates sustained through the contraction.

The computed average energy dissipation from within the contraction for each of the experimental flow rates compared to the corresponding observed relative damage for *H. bacteriophora*, *H. megidis*, *S. carpocapsae*, and *S. glaseri* are given in Figure 7. Appreciable damage starts to be observed at average energy dissipation levels of 1.23E + 8 W/m^3 for *H. bacteriophora*, 1.72E + 8 W/m^3 for *H. megidis*, 2.89E + 8 for *S. glaseri*, and 3.70E + 8 W/m^3 for *S. carpocapsae*. As the energy dissipation rate increases, the level of relative damage increases. The rate of relative damage increase with energy dissipation, upon observation, appears to be similar for the four species. Based on this information, energy dissipation rates within an equipment component should be kept below approximately 1E + 8 W/m^3 to avoid hydrodynamic related EPN damage.

DISCUSSION

Since the intent of this work was to fundamentally study the extent and pattern of damage to EPNs within a contraction flow field, quantitative observations after treatment were reasonable. Presently, nematode viability is most commonly being assessed using microscopic examination, where movement, when probed if necessary, is the key criterion for survival. Some studies have reported using methylene blue as a staining agent, where nonviable nematodes are stained blue and viable nematodes remain colorless (Chavarria-Hernandez et al., 2003). Still, the use of a light microscope is necessary for quantification of the viability. More sophisticated techniques have been used to quantify cellular damage, namely chemical assay (Al-Rubeai et al., 1995; Ma et al., 2002). To the authors' knowledge, similar sophisticated techniques for damage assessment of EPNs have not been developed, but certainly would be worthwhile investigating in future studies.

The consideration of half and quarter pieces for calculation of nematode relative damage [Eq. (5)] is reasonable with respect to well-established theory, which states that for a flow field with a uniform velocity gradient, a fully extended body will experience a ''stretching'' force that is maximal at the center of the body (Levinthal and Davison, 1961). Thus, if the force becomes large enough, a body would be expected to disrupt at or near its center. Further, it is reasonable that a half piece could break at or near its center into two quarter pieces. The nematodes were modeled as fully extended rods within the experimental flow field. Therefore, the approximately ''half'' and ''quarter'' pieces of nematodes that were consistently observed in the experiments are meaningful with respect to the flow theory.

The long, slender shape of the EPNs required local flow field analysis using information from the FLUENT simulations. As the contraction diameter was similar to the length of the EPNs, the EPN's longitudinal axis had to be aligned with the flow for the nematodes to pass through the contraction. The absence of appreciable EPN damage at volumetric flow rates less than 14.87 cm^3/s indicates that the EPNs were able to pass through the contraction without difficulty, which supports the assumption that the nematodes were fully extended and aligned with the flow.

A fast-transient tensile stress field occurs in the region near the contraction entrance. For flow along the central streamlines, the EPNs experienced maximum tensile stress when they were centered at the location of maximum σ_{zz} (Fig. 5a). At this point, the EPNs were essentially loaded with a tensile stress for a very short period of time. With respect to the tensile loading, the observed ''necking'' phenomenon (Fig. 3) can be explained by classic mechanics of

materials. For a solid cylinder, at an ultimate tensile stress the cross-sectional area will begin to decrease at the geometric center causing a neck to form. The necking will continue until a fracture stress is reached at which point failure of the material occurs. Broken pieces of *Heterorhabditis* nematodes were observed in some cases, particularly under more intensive flow conditions, which is indicative of the fracture stress being reached. The observations on how the *Heterorhabditis* nematodes were damaged supports the hypothesis suggested by several researchers (Croughan and Wang, 1989; Garcia-Briones and Chalmers, 1994; Gregoriades et al., 2000; McQueen et al., 1987) that the extensional flow regime is more damaging to a body than purely shear flow. The necking region that formed, and consequently became lethal to the *Heterorhabditis* nematodes, was only possible due to the effects of a tensile stress, which characterizes an extensional flow regime.

The fast-transient nature of the contractional flow also results in a relaxation of the tensile stress. The processes of tensile stress loading and relaxation may provide insight into the differences in damage response observed for the *Heterorhabditis* nematodes compared to *Steinernema*. The mechanism responsible for causing the internal rupture of the *Heterorhabditis* nematodes remains unclear, however it is speculated that at some point between the processes of stretching and relaxation the intestine was disrupted and the nematode was fatally damaged. This type of damage was not observed for *S. carpocapsae* and *S. glaseri*. Thus, *H. bacteriophora* and *H. megidis* may have structural membrane properties that are more elastic than *S. carpocapsae* and *S. glaseri* such that at moderate flow conditions (i.e., <28.09 cm^3/s) these EPNs were stretched and relaxed to a greater extent causing the internal disruption.

Knowledge of the structural properties of EPNs is needed to understand how the organism will respond to hydrodynamic stress. The cuticle ultrastructure of the infective juvenile (IJ) stage has been evaluated for several *Steinernema* spp., including *S. carpocapsae* and *S. glaseri* (Kondo and Ishibashi, 1989; Patel and Wright, 1998). *Steinernema carpocapsae* has a proportionately greater striated layer in the cuticle of IJs compared to several other *Steinernema* spp. (Kondo and Ishibashi, 1989; Patel and Wright, 1998). Kondo and Ishibashi (1989) indicate that the importance of the striated layer is to provide structural support to the nematode cuticle. The enhanced structural integrity of *S. carpocapsae* compared to *S. glaseri* provides an explanation for the ability of *S. carpocapsae* to withstand higher levels of hydrodynamic stress before appreciable damage was observed. Even for the highest flow rate tested, *S. carpocapsae* only had 50% relative damage compared to over 90% damage for the other species. At present, there is no information available on the cuticle ultrastructure of *H. bacteriophora* or *H. megidis*. This information is essential for better understanding of the differences in how the EPNs from Heterorhabditidae and Steinernematidae families are damaged due to hydrodynamic stress.

Entomopathogenic nematodes are categorized by their host-seeking behavior (i.e., ambusher or cruiser). Ambushers perform a behavior referred to as nictation, where the EPNs stand on their tails and alternately wave their body from side to side and then pause in a straight extended state. Active nictators include *S. carpocapsae* and *S. scapterisci* (Grewal and Georgis, 1999; Ishibashi and Kondo, 1990). Cruising EPNs do not nictate, but rather they are highly mobile. Cruisers include *H. bacteriophora*, *H. megidis*, and *S. glaseri* (Grewal and Georgis, 1999). With regard to *S. carpocapsae*, Kondo and Ishibashi (1989) suggested that the thicker striated layer was important for nictation in providing structural support to the body during this activity. Entomopathogenic nematodes that actively nictate have enhanced structural properties that may allow them to withstand greater levels of hydrodynamic stress. Thus, host-seeking behavior may be a way to categorize EPN sensitivity with respect to hydrodynamic related damage. The significantly lower relative damage of *S. carpocapsae* (ambusher) observed in the current study compared to *H. bacteriophora*, *H. megidis*, and *S. glaseri* (all cruisers) supports this concept.

Recent advances in micromanipulation techniques have made it possible to measure the ultimate tensile strength of biological materials, however, this technology is still at early stages of development (Thomas and Zhang, 1998). Wilson et al. (2001) used calibrated weights hung from a micro-wire attached to one end of an adult nematode to measure the average tensile force required to break the nematode, which was found to be approximately 5E-2 N. No specific nematode was mentioned for this test, but *H. megidis* and *Phasmarhabditis hermaphrodita* were used in other parts of their study. The tensile force values associated with nematode damage that were computed in the current study (Table III), for the infective juvenile (IJ) stage (J3), were considerably smaller than observed by Wilson et al. (2001) for an adult nematode. This result was unexpected because it has been reported that young juvenile stages (J1–J3) of nematodes are less sensitive to shear stress than adult nematodes (Friedman, 1990). However, Wilson et al. (2001) measured the tensile force required to cause complete failure of the nematode structural membrane, while the values in this study represent tensile forces that can cause enough damage to be lethal to a nematode. In a recent study, Chavarria-Hernandez et al. (2003) reported that among the different developmental stages of nematodes, only juveniles of the first stage (J1) were highly susceptible (85% reduction in viability) to the shearing conditions they tested, which is in contrast to previous work (Friedman, 1990). Clearly, more research is necessary to evaluate the mechanical properties of EPNs from, not only different species, but also different developmental stages to clarify these differences in observations.

Changes in pressure occur during flow into a contraction. Fife et al. (2003) evaluated the effect of pressure differentials on several EPN species and found that the relative

damage of the treated EPNs remained below 15% for pressure differentials up to 1283 kPa for *H. megidis* and 2183 kPa for *H. bacteriophora* and *S. carpocapsae*. In the current study, for experimental conditions when appreciable damage started to be observed, the total pressure changes within the contraction were less than 600 kPa (Table III), which is well below the levels cited by Fife et al. (2003) for damage due to a pressure differential. Thus, it is reasonable to assume that the changes in pressure within the flow field were not large enough to contribute to the observed EPN damage.

Using the same contraction flow device that was used in the current study, Gregoriades et al. (2000) observed detectable damage of a microcarrier culture of cells at total maximum energy dissipation rates of 10^3 W/m^3 and considerable cell damage (>40%) at 10^6 W/m^3. In the current study, appreciable EPN damage was observed at average energy dissipation rates of 10^8 W/m^3 and greater (Fig. 7), which is over two orders of magnitude larger than the levels reported by Gregoriades et al. (2000). However, Gregoriades et al. (2000) indicted that from experimental observations cells attached to microcarriers are more susceptible to hydrodynamic damage than suspended cells. Recently, Ma et al. (2002) tested four animal cell lines (including CHO-K1, the same cell line evaluated in Gregoriades et al., 2000) in a microfluidic contraction flow device and found that the suspended cells were able to withstand relatively intense energy dissipation rates. The maximum local energy dissipation rates where appreciable damage started to be observed varied between approximately 7E + 7 W/m^3 and greater than 2E + 8 W/m^3 for these four cell lines. These values are similar to the average energy dissipation rates determined in the current study for EPNs. Also, the trends were consistent with current results in that the relative damage remained low until a certain level of energy dissipation and then increased rapidly.

CONCLUSIONS

The results from this study provide basic information on how and to what degree the EPNs were damaged during flow through an abrupt contraction, a predominately extensional flow regime. Evaluation of the stress tensor components from the central streamline showed that during entrance into the contraction a fully extended EPN could, momentarily, experience a tensile loading large enough to cause damage. The relative elasticity of the EPN structural membrane may explain the differences in damage observed between the species. The internal ruptures observed within *H. bacteriophora* and *H. megidis* most likely occurred sometime during the process of stretching and relaxation during flow through the contraction entrance. The cuticle ultrastructure properties of *S. carpocapsae* are known to be more robust than other EPN species, which supports the observation that *S. carpocapsae* was able to withstand more intensive hydrodynamic conditions compared to the other EPN species evaluated. In general, energy dissipation rates within an equipment component should be kept below 1E + 8 W/m^3 to avoid hydrodynamic related EPN damage. Comparison of the average energy dissipation and EPN damage provides important benchmark information for future evaluation of flow conditions within actual agricultural spray equipment components.

The authors offer special thanks to Dr. Kurt Koelling from the Department of Chemical Engineering at The Ohio State University for use of the contraction flow device, Andy Doklovic for technical assistance in experimental setup, and Leslie Morris and Leona Horst for technical assistance with the scanning electron microscope.

References

Al-Rubeai M, Singh RP, Goldman MH, Emery AN. 1995. Death mechanisms of animal cells in conditions of intensive agitation. Biotechnol Bioeng 45:463–472.

Bateman RP. 1999. Delivery systems and protocols for biopesticides. In: Hall FR, Menn JJ, editors. Methods in biotechnology, vol. 5: Biopesticides use and delivery. Totowa, NJ: Humana Press. p 509–528.

Bluestein M, Mockros LF. 1968. Hemolytic effects of energy dissipation in flowing blood. Med Biol Eng 7:1–6.

Chisti Y. 1999. Shear sensitivity. In: Flickinger MC, Drew SW, editors. Encyclopedia of bioprocess technology: Fermentation, biocatalysis, and bioseparation, vol. 5. New York: Wiley. p 2379–2406.

Clay JD, Koelling KW. 1997. Molecular degradation of concentrated polystyrene solutions in a fast transient extensional flow. Polym Eng Sci 37:789–800.

Chavarria-Hernandez N, Rodriguez-Hernandez AI, Perez-Guevara F, de la Torre M. 2003. Evolution of culture broth rheological properties during propagation of the entomopathogenic nematode *Steinernema carpocapsae*, in submerged monoxenic culture. Biotechnol Prog 19: 405–409.

Copping LG, Menn JJ. 2000. Biopesticides: A review of their action, applications and efficacy. Pest Manag Sci 56:651–676.

Croughan MS, Wang DI. 1989. Growth and death in overagitated microcarrier cell cultures. Biotechnol Bioeng 33:731–744.

Fife JP, Derksen RC, Ozkan HE, Grewal PS. 2003. Effects of pressure differentials on the viability and infectivity of entomopathogenic nematodes. Biol Control 27:65–72.

Friedman MJ. 1990. Commercial production and development. In: Gaugler R, Kaya HK, editors. Entomopathogenic nematodes in biological control. Boca Raton, FL: CRC Press. p 153–172.

Garcia-Briones MA, Chalmers JJ. 1994. Flow parameters associated with hydrodynamic cell injury. Biotechnol Bioeng 44:1089–1098.

Gaugler R, Grewal P, Kaya HK, Smith-Fiola D. 2000. Quality assessment of commercially produced entomopathogenic nematodes. Biol Control 17:100–109.

Gregoriades N, Clay J, Ma N, Koelling K, Chalmers JJ. 2000. Cell damage of microcarrier cultures as a function of local energy dissipation created by a rapid extensional flow. Biotechnol Bioeng 69:171–182.

Grewal P, Georgis R. 1999. Entomopathogenic nematodes. In: Hall FR, Menn JJ, editors. Methods in biotechnology, vol. 5: Biopesticides use and delivery. Totowa, NJ: Humana Press. p 271–299.

Ishibashi N, Kondo E. 1990. Behavior of infective juveniles. In: Gaugler R, Kaya HK, editors. Entomopathogenic nematodes in biological control. Boca Raton, FL: CRC Press. p 139–150.

Joshi JB, Elias CB, Patole MS. 1996. Role of hydrodynamic shear in the cultivation of animal, plant and microbial cells. Chem Eng J 62: 121–141.

Kaya HK, Stock SP. 1997. Techniques in insect nematology. In: Lacey LA, editor. Manual of techniques in insect pathology. London: Academic Press. p 281–324.

Kondo E, Ishibashi N. 1989. Ultrastructural characteristics of the

infective juveniles of *Steinernema* spp. (Rhabditida: Steinernematidae) with reference to their motility and survivial. Appl Entomol Zool 24:103–111.

Kresta S. 1998. Turbulence in stirred tanks: Anisotropic, approximate, and applied. Can J Chem Eng 76:563–576.

Levinthal C, Davison PF. 1961. Degradation of deoxyribonucleic acid under hydrodynamic shearing forces. J Mol Biol 3:674–683.

Ma N, Koelling KW, Chalmers JJ. 2002. Fabrication and use of a transient contractional flow device to quantify the sensitivity of mammalian and insect cells to hydrodynamic forces. Biotechnol Bioeng 80:428–437.

Mardikar SH, Niranjan K. 2000. Observations on the shear damage to different animal cells in a concentric cylinder viscometer. Biotechnol Bioeng 68:697–704.

McQueen A, Meilhoc E, Bailey JE. 1987. Flow effects on the viability and lysis of suspended mammalian cells. Biotech Lett 9:831–836.

Nilsson U, Gripwall E. 1999. Influence of application technique on the viability of biological control agents *Verticillium lecanii* and *Steinernema feltiae*. Crop Prot 18:53–59.

Patel MN, Wright DJ. 1998. The ultrastructure of the cuticle and sheath of infective juveniles of entomopathogenic Steinernematid nematodes. J Helmin 72:257–266.

Poinar GO, Jr. 1990. Taxonomy and biology of Steinernematidae and Heterorhabditidae. In: Gaugler R, Kaya HK, editors. Entomopathogenic nematodes in biological control. Boca Raton, FL: CRC Press. p 23–61.

Schlichting H. 1955. Boundary layer theory. New York: McGraw-Hill. 647 p.

Tadmor Z, Gogos CG. 1979. Principles of polymer processing. New York: Wiley.

Thomas CR, Zhang Z. 1998. The effect of hydrodynamics on biological materials. In: Galindo E, Ramirez OT, editors. Advances in bioprocess engineering II. The Netherlands: Kluwer Academic Pub. p 137–170.

Wilson JA, Pearce JD, Shamlou PA. 2001. Scalable downstream recovery of nematodes used as biopesticides. Biotechnol Bioeng 75:733–740.